Microstructure Evolution during Near-net-shape Fabrication of Ni_xAl_y-TiC Cermets through Binder Jet Additive Manufacturing and Pressureless Melt Infiltration

Joshua M. Arnold[1,4], Corson L. Cramer[2,*], Amy M. Elliott[2], Peeyush Nandwana[3], Sudarsanam Suresh Babu[3,4]

[1]Arconic Engines, Midway, GA, USA 31320

[2]Energy and Environmental Sciences Directorate, Oak Ridge National Laboratory, Oak Ridge, TN, USA 37830

[3]Materials Science and Technology Division, Oak Ridge National Laboratory, Oak Ridge, TN, USA 37830

[4]Department of Mechanical, Aerospace, and Biomedical Engineering, The University of Tennessee, Knoxville, TN 37996

*cramercl@ornl.gov

Abstract

Titanium carbide-nickel aluminide (TiC-Ni_xAl_y) intermetallic matrix composite materials were fabricated with additive manufacturing and pressureless melt infiltration for applications intended for high-wear and corrosive environments while maintaining low density. Here, two compositions of nickel aluminide are infiltrated into porous, printed TiC preforms. Net shaping of a nickel-rich infiltrant is less compared to the net shaping of the aluminum-rich infiltrant due to dissolution of TiC in the molten infiltrant. The microstructures and porosity of the two infiltrants with TiC are examined after processing. The explanation of shape retention from infiltration is explained, and the excellent shape retention in an Al-rich infiltrant system is thought to be from peritectic behavior and a metered infiltration of different phases during cooling and solidification without significant dissolution. The metered infiltration contributed to some porosity, microcracking, and segregated Ni_xAl_y phases. This work demonstrates that TiC can be shaped and infiltrated with intermetallics to provide a method of making composites with limited shrinkage and controlled geometry.

Key Words: Intermetallic matrix composites, Pressureless melt infiltration, Ni_xAl_y-TiC composite

1 Introduction

Metal matrix composite (MMC) materials provide unique properties that combine those of metallic materials (e.g. ductility, toughness) with those of ceramic materials (e.g. high strength, stiffness, and hardness) [1], [2]. By combining metals and ceramics, materials can be created that exceed the properties of either of the individual phases. MMCs based on intermetallic matrices have received considerable interest due to the attractive properties that often includes excellent corrosion resistance, low densities, and the ability to retain strength at elevated temperatures [3]–

[8]. Ashby extended this MMC formulism and introduced the notion of dispersing two phases in different geometric forms and referred to this new class of materials as hybrid materials [9]. In this paper, the authors explore the possibility of forming hybrid materials with the Ni-Al binary system that include both intermetallic phases as a ductile matrix with binder jet additive manufacturing to make intermetallic matrix composites (IMCs).

1.1 Ni-Al Intermetallics

Intermetallic phases of the Ni-Al binary system, known as nickel aluminides, have been researched extensively [10]. The Ni-rich phases Ni_3Al and NiAl have high melting points and ordered crystal structures that allow these compounds to retain strength at elevated temperatures making them excellent candidates for high-temperature structural applications. Ni_3Al, also known as γ', is the primary strengthening phases in most nickel superalloys and has great potential in MMCs and IMCs as a matrix material [5], [6], [11]. Ni_3Al has excellent properties; however, it does have some drawbacks – primarily, poor ductility at room temperature and a brittle intergranular fracture mechanism [10]. Addressing such problems has been an important research focus over the past several decades and has largely been addressed by different alloying additions including B and Cr [5], [12].

The Ni-rich intermetallic phases of the Ni-Al binary system have certainly received the most interest, but there also exists an Al-rich intermetallic in the same binary system: $NiAl_3$. This compound has a very small presence in literature, which is likely because it does not have a high melting point or ordered crystal structure like its Ni-rich counterparts. However, while $NiAl_3$ may not be attractive for high-temperature structural applications, it may be a potential candidate material for lightweight tooling, wear resistance, and aerospace applications due to its low density of 3.96 g/cc and complex crystal structure that gives the metal its high hardness [13], [14].

While nickel aluminides may individually have attractive properties that warrant their use in a wide array of applications, there may also be a great benefit in using these compounds as a matrix of binder phase in IMCs. Reinforcing Ni_3Al with TiC will reduce the overall weight of the material while also increasing the strength and stiffness of the material. Conversely, TiC may be added to $NiAl_3$ that will result in only a small increase in overall weight but provide increased wear resistance.

1.2 Near Net Manufacturing of Ni-Al IMCs

Nickel aluminide IMCs can be fabricated by several different processing methods, but near-net-shape fabrication may be particularly beneficial. Firstly, Ni_3Al is a work hardening material and, combined with the inherently high wear resistance of cemented nickel aluminides, these materials are difficult to machine [15]. Secondly, the potential need for more complex geometries in tooling applications can drive the cost of machining even higher. TiC-reinforced nickel aluminide cermets have been produced by a myriad of processing methods including powder metallurgy [16]–[20], liquid-state processing such as melt infiltration [21]–[27], and in-situ sintering methods [26], [28]–[31]. While net-shaping of Ni_xAl_y-TiC composites may be

achieved by powder metallurgy techniques, these methods rely on densification by shrinkage during sintering and, as such, are not directly applicable to the near-net-shape fabrication methods presented within. Melt infiltration techniques, however, achieve densification by filling void porosity rather than shrinkage and, thus, are complimentary with binder jet additive manufacturing.

Plucknett and Becher first demonstrated a melt infiltration technique for Ni_3Al-TiC composites where Ni_3Al pellets were set on top of a TiC preform prepared using cold isostatic pressing (CIP). The pellets were melted and liquid Ni_3Al wicked downward into the TiC preform driven by both capillary and gravitational forces to achieve near full density. When enough Ni_3Al to fill the entire void space of the preform was used, consolidation was achieved by filling the void porosity (infiltration). When lesser amounts of Ni_3Al were used, both filling of void porosity and liquid phase sintering of the TiC preform provided consolidation (infiltration-sintering). Notably, Plucknett and Becher showed that when filling void porosity dominated densification, the linear shrinkage of the composite was <7%, low enough to be considered near-net-shape [21], [22], [24]. Pan et. al reported a similar process to Plucknett and Becher's in which a TiC preform was prepared by P/M; however, the Ni_3Al powder was placed below the TiC preform. By doing so, an "upward" infiltration was achieved where liquid metal wicked up into the TiC preform driven purely by capillary action. For equal volume fractions of Ni_3Al metal, Pan reported faster infiltration times (20 min for a 4 mm thick sample) and higher mechanical properties including flexural strength and fracture toughness. Pan attributed these observations to the uni-directional infiltration front that occurs during the upward infiltration process as opposed to the multi-directional infiltration front in Plucknett and Becher's method. In the case of multiple infiltration fronts, defects occur such as solute pinning or gas porosity getting trapped at the intersection points. The advantages of an upward infiltration front were demonstrated in terms of lowered processing times and increased mechanical properties [23]. Additionally, an upward infiltration method lends itself to the use of preforms that have more complex geometries where the preform can be placed on a bed of metal powder/pellets regardless of shape. While the above-described methods may provide near-net-shape fabrication, geometry and shape of the TiC preform is limited to what the P/M preparation methods may provide.

More recently, Collier and Plucknett have described a similar melt infiltration process for fabricating Ni_3Al-TiC composites, but the TiC preform is prepared via an aqueous slip casting procedure. A TiC suspension is directionally slip cast into cylindrical molds to form the preform shape, after which the preforms are pressureless infiltrated using the same procedure described by Plucknett and Becher [25]. The use of a casting mold might allow for more complex geometries than traditional powder metallurgy methods could supply, although cost may be a factor as design complexity increases. Additionally, casting molds may have difficulty with preparing organically shaped designs.

It is clear from studying literature that there is no present methodology for the near-net-shape fabrication of Ni_xAl_y-TiC cermets with complex geometries. To address this need, the authors explored fabricating more complex geometries in a cost-effective manner using binder jet additive manufacturing. TiC preforms were fabricated by binder jet additive manufacturing and then upward melt infiltrated to incorporate the nickel aluminide binder. The use of binder jet additive manufacturing, as mentioned briefly above, is an excellent fabrication method for

cemented carbide cermet materials. One of the current drawbacks of binder jet additive manufacturing is the low print density (<50%) of the fabricated preforms, which means that in order to consolidate to full density by traditional sintering methods, the preforms experience a significant amount of shrinkage and compromise the near-net-shape capability. This makes the fabrication of metal alloys difficult. Conversely, the porous preforms may also be consolidated to full density by filling the void porosity of the preform with a second, lower-melting point phase that does not experience the same shrinkage and preserves the net-shape capability of the process. Inherently, this makes intermetallic matrix composites a compatible material type with binder jet additive manufacturing. By combining binder jet additive manufacturing with an upward infiltration process, Ni_xAl_y-TiC cermets may be fabricated in a near-net-shape fashion with the potential for complex geometries that is also cost-effective.

2 Experimental Procedure

2.1 Manufacturing Methods

Porous TiC preforms were made using an X1-Lab binder jet printer from ExOne shown in Fig. 1. The dimensions of the preforms were 15 × 15 × 10 mm with an inner cavity that measured to be 10 × 10 × 5 mm such that the total material volume was ~1.75 mm^3. A cubic cup geometry was chosen because it is a simple geometry that also contains features of varying thickness (i.e. the walls versus the base of the cup). The challenge was that even if the overall part experiences little shrinkage during processing, the near-net-shape capability of the process depends on the thin-wall features maintaining a set profile.

The printing parameters (shown in Table 1) were as follows: layer thickness of 100 μm, binder saturation of 85%, powder packing ratio varied from 35–40% between prints, dryer intensity of 90% with a dryer pass time of 16 s for a build plate width of 40 mm. De-powdering the TiC preforms after completion of the build cycle was done by hand with a small brush. To prepare the TiC preforms for further processing, the adhesive binder must first be burned off. De-binding the preforms was done in a Neytech bench top furnace with the following furnace cycle: preforms were heated at 10°C/min to 630°C, held for 1.5 h, heated at 10°C/min to 900°C and held for an additional hour, and then cooled to room temperature at 10°C/min. Following the binder burnout, the porous TiC preforms had a “green” density of ~30%, measured by taking dimensional measurements of the cup to determine total volume and dividing by the weight.

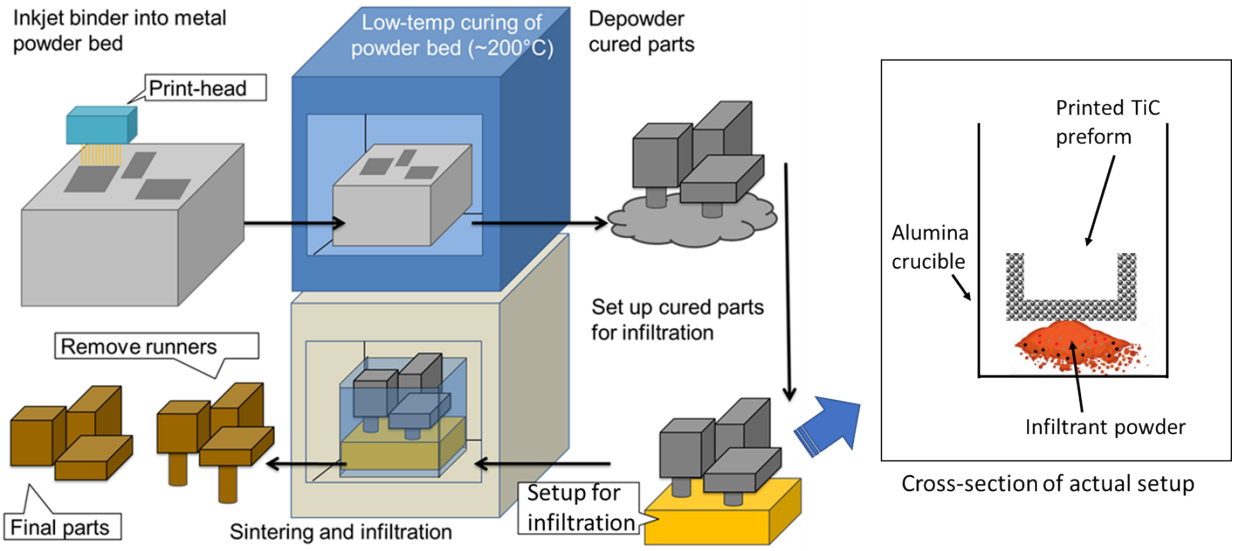

Figure 1. Cermet process flow for binder jet additive manufacturing and melt infiltration processing [32].

Table 1. Process parameters for infiltration experiments. Atmosphere of Ar-4% H_2.

Sample #	Print Density (% TD)	Debind Temperature and Time (ºC, h)	Sintering Temperature and Time (ºC, h)	Infiltrant	Infiltration Temperature (ºC)	Time (min)	Heating Rate (ºC/min)
1	n/a	1400, 2		Ni_3Al	1430	30	10
2	30	1400, 2		Ni_3Al	1430	15	10
3	n/a	900, 1	1450, 2	$NiAl_3$	1415	30	6.67

2.2 Powder Materials

Preforms were printed using TiC powder (-325 mesh) purchased from Atlantic Equipment Engineers (AEE), designation Ti-301. The average particle size varied from ~2–30 µm between batches and was measured using a Malvern Panalytical Morphologi G3 microscope. The powder size distribution and powder morphology are shown Fig. 2.

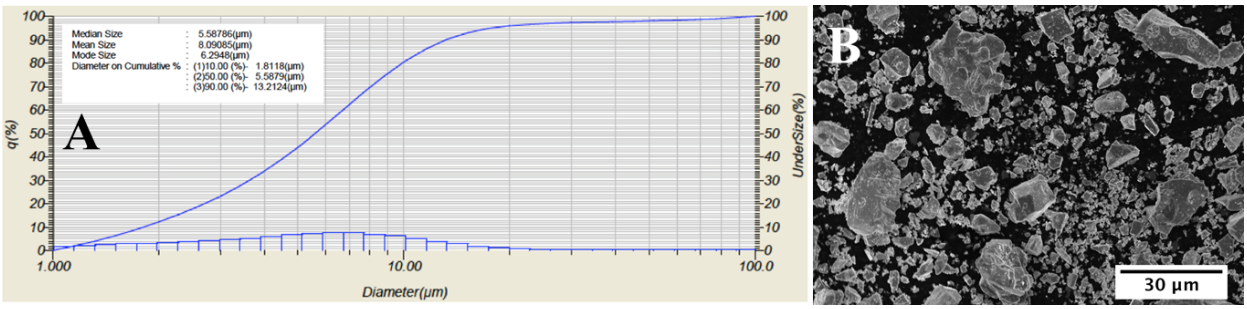

Figure 2. A) Laser scattering powder distribution analysis performed using Horiba LA-950 Ver. 6 software. B) Scanning electron microscopy image of -325 mesh AEE TI-301 TiC powder, 1000×.

Ni_3Al powder for infiltration was purchased from AEE, designation Ni-305 with a -325 mesh powder distribution. Unmarked $NiAl_3$ from previous experiments at Oak Ridge National Laboratory were used. The chemical composition of the two nickel aluminide powders was measured by direct current plasma spectroscopy in accordance with ASTM E1097-12 and is shown in Table 2.

Table 2. Chemical composition of Ni_3Al and $NiAl_3$ powders in wt.%

Infiltrant	Ni	Al	Zr	Cr	Mo	Ca	Fe	Si	Ti	W
Ni_3Al	84.8	14.1	0.2	0.075	0.11	<0.01	0.17	0.24	0.028	0.17
$NiAl_3$	41.2	58.1	0.0057	0.30	0.002	0.023	0.054	<0.01	0.3	0.054

2.3 Material Characterization

Characterization of the infiltrated specimens focused on both the macro and microstructures of the composite. Optical microscopy was used to assess the overall macro cross-section of the infiltrated specimen to assess the infiltration behavior of the liquid penetrant into the porous TiC preform. Scanning electron microscopy (SEM) and energy dispersive X-ray spectroscopy were used to analyze the microstructure and composition of the infiltration specimens with specific emphasis on the metal/ceramic interface. Phase analysis of the infiltrated preforms was done by X-ray diffraction characterization (XRD) using a PANalytical Xpert Diffractometer with continuous 2θ scans from 5–60°. Mo-Kα radiation (λ=1.541838Å) was used to prevent fluorescence of Ni within the samples. To better understand the structure of the printed TiC preform and the overall particle arrangement, X-ray computed tomography characterization was performed on the printed TiC preforms using a Zeiss Xradia Versa. The preforms were rotated 360° around the vertical axis while images were taken at equal rotational intervals. A 0.4× wide field of view (FOV) scintillator objective was used and attached to a camera capturing a 21 mm diameter FOV. A 1×1 camera binning was used, yielding a pixel size of 11.183 μm.

3 Results

3.1 TiC Arrangement in As-Printed Preform

Fig. 3 shows a macro-image and CT scan of the printed and sintered TiC preform. Print densities

were near ~30% theoretical density (TD). The low density of the printed preforms may partially result from using TiC with a fine particle size, which has poor flowability, compared to larger particle sizes. A fine particle size may also hinder the binder from fully penetrating individual layers, indicated by the sporadic gaps or holes in the preform. A cross-sectional image of the XCT scan performed on the preform is shown in Fig. 3B, where TiC particles (grey) are visibly arranged in a dimensionally connected network structure. XCT shows the arrangement of TiC particles in the green state of the preform prior to infiltration. Even though the preform is heated to increase density prior to infiltration, little to no densification of the preform was observed. The resolution limit of the XCT scan is ~10 μm while the average particle size of TiC powder used in this print was ~2.5 μm so the grey areas likely represent TiC particle clusters rather than individual particles.

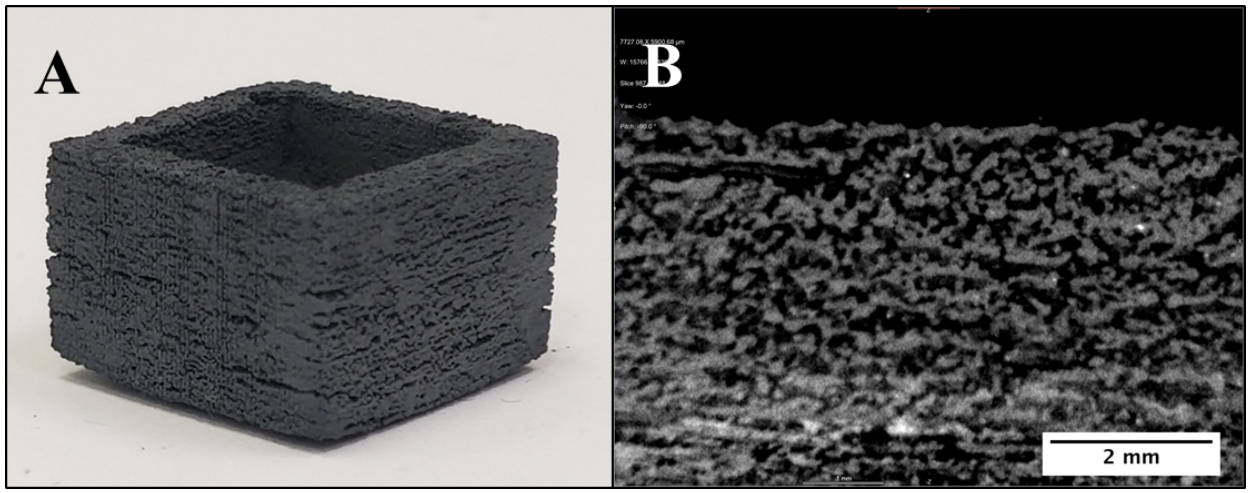

Figure 3. A) Printed TiC preform, ~30% dense, 15 mm × 15 mm × 10 mm outer dimensions. 5 mm × 5 mm × 7.5 mm inner cavity dimensions. B) XCT of TiC preform (~30% dense), sintered at 1500°C for 2 h. Resolution is ~10 um. Average particle size is ~2.5 μm.

3.2 Ni_3Al Infiltrated TiC Preforms

Fig. 4 shows macro images and one optical cross-section of the TiC preform infiltrated with Ni_3Al at 1430°C for 30 min with ~8 wt.% excess infiltrant supplied. There is full volumetric infiltration of the TiC preform but with very poor shape retention. The thin walls of the preform partially collapsed and the base of the preform appears to have partially dissolved in the liquid metal, likely a result of TiC dissolution by liquid Ni_3Al, also noted by [20], [24], [26], [30], [33]. Dissolution of the preform base is also possibly amplified by the amount of excess infiltrant that might remain after full saturation of the preform by the liquid or if the sample were to initially sink into the melt pool. Noticeably, upward flowing traces of the liquid infiltrant exist around the outside of the preform, a phenomenon documented by Pan as an indicator of the strong driving force for Ni_3Al into the TiC preform [23]. Fig. 4C shows a cross-section of the infiltration specimen that revealed solid Ni_3Al metal fused around the base of the preform, which contains a significant amount of porosity. The density of the infiltrated preform was measured to be ~95% by the Archimedes method, but this includes the excess pure metal fused to the outside of the preform.

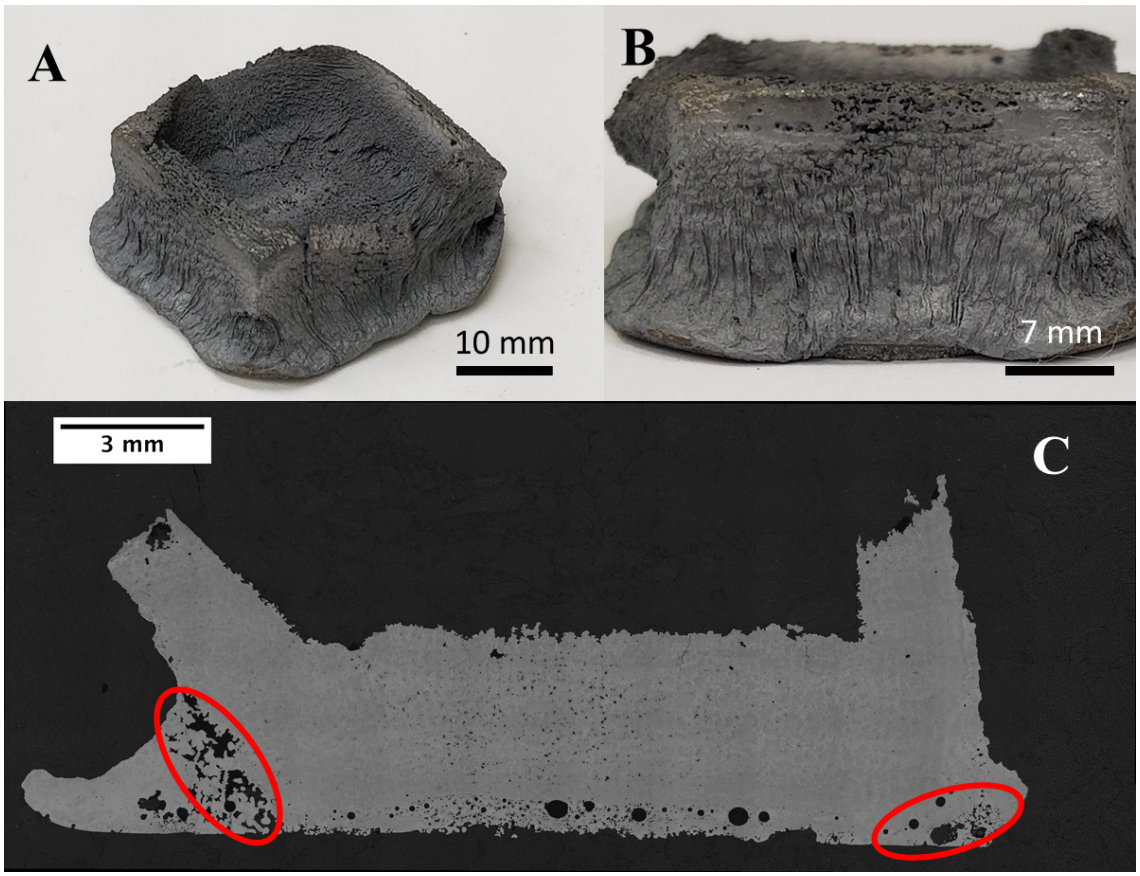

Figure 4. A) and B) TiC preform infiltrated with Ni_3Al at 1430°C for 30 min. Visibly poor shape retention. C) Optical stitching of infiltrated preform.

Fig. 5 shows the optical and SEM microstructure of the Ni_3Al-infiltrated preform. SEM in Fig. 5B revealed a rough, uniform dispersion of TiC particles within a Ni_3Al matrix similar to what might be seen in a traditional P/M fabricated microstructure with no evidence for the structural network of TiC particles in the as-printed state of the preform. However, low-mag optical microscopy in Fig. 5A revealed subtle clusters of TiC particles within the overall dispersion of TiC, indicating that the network structure of the original TiC preform is at least partially preserved after infiltration by Ni_3Al. Closer inspection of the infiltrated preform revealed a small amount of micro-porosity near the center of the preform that appears to be contained within the remaining TiC clusters. The apparent lack of porosity away from the center of the preform is a good indicator that the liquid Ni_3Al penetrated and broke apart the TiC clusters. It also appears that the center of the preform was the last to be impregnated by liquid Ni_3Al. During the infiltration process, liquid Ni_3Al infiltrated the micro-capillaries that exist between the TiC particles that make up the larger clusters where heavy dissolution of TiC by liquid Ni_3Al forced the clusters to break apart and, thus, the overall network structure was lost and the preform could no longer maintain a net shape.

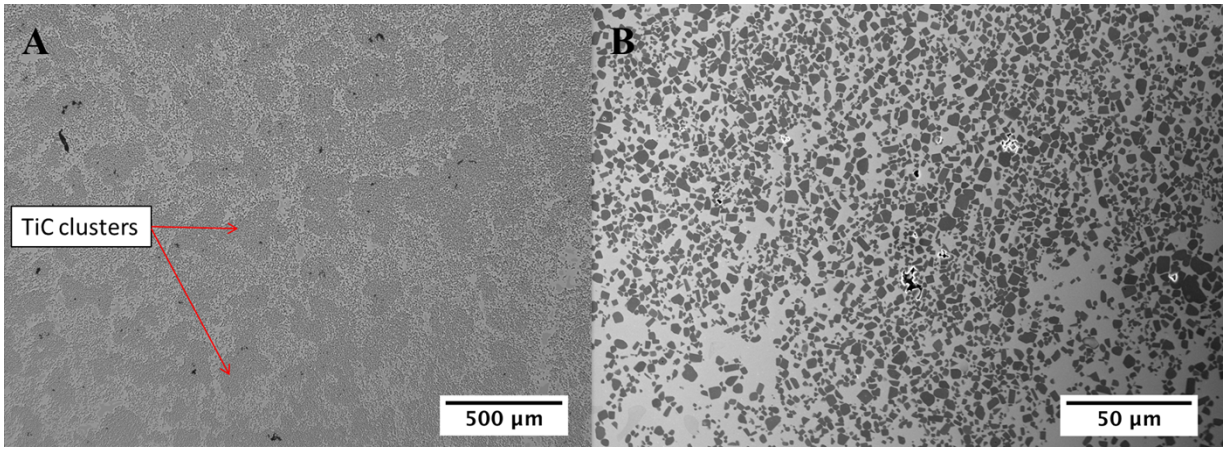

Figure 5. A) Optical micrograph reveals clusters of TiC still present in microstructure. 5×. TiC preform infiltrated by Ni_3Al for 30 min at 1430°C. B) SEM image of TiC preform infiltrated by Ni_3Al at 1430°C for 30 min. 500×.

3.3 $NiAl_3$ Infiltration of Printed TiC Preforms

Fig. 6 shows macro images and an optical cross-sectional image of the TiC preform infiltrated by $NiAl_3$ at 1415°C for 30 min with ~70 wt.% excess infiltrant powder supplied to allow for complete infiltration. The full volume of the preform was infiltrated by $NiAl_3$ and exhibits excellent shape retention (see Fig. 6A and B); the thin walls of the cubic cup retained their structural integrity and the bottom of the preform is intact. The total shrinkage after infiltration was measured to be <2% in any single direction. However, a significant amount of porosity was present after infiltration and the infiltrated preform was measured to be ~88–90% TD by the displacement method. Additionally, cracking behavior was observed within the material and shows the brittle nature of the alloy. Fig. 6C shows the cracking and porosity. During previous infiltration of the TiC preform by Ni_3Al, the infiltrant exhibited clear melting behavior and any excess material that did not penetrate the TiC preform was observed to be fused around the outside of the preform after infiltration and cooling. However, after attempted infiltration by $NiAl_3$ and despite the large amount of present porosity within the infiltrated preform, a solid mass of material remained in the crucible as in Fig. 6B, the infiltrant did not exhibit a clear melting behavior, and significant porosity was visible throughout the preform. A cross-section was taken through the center of the preform where small warpage at corners was not discernable.

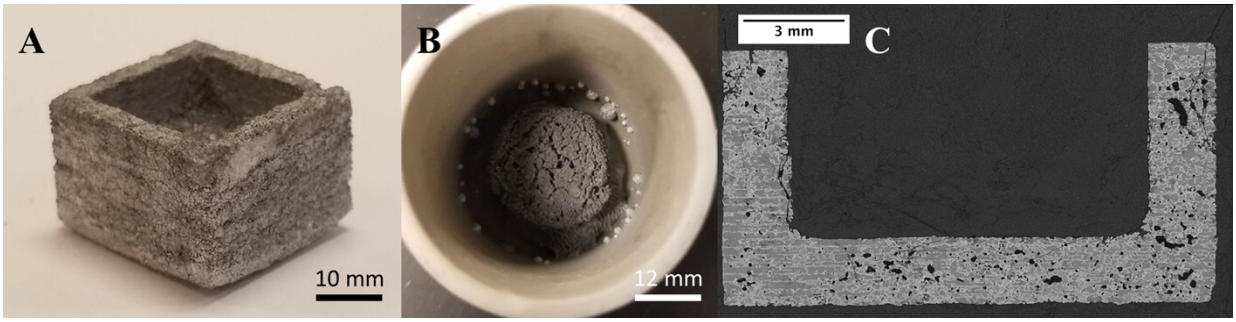

Figure 6. A) TiC preform infiltrated by $NiAl_3$ at 1415°C for 30 min. Preform shows excellent shape retention. B) Remnant material in crucible after infiltration. Dark phase exhibits no clear melting behavior. C) Optical image of TiC preform infiltrated by $NiAl_3$ at 1415ºC for 30 min.

Fig. 7 shows the microstructure of the TiC preform infiltrated by $NiAl_3$ at 1415°C for 30 min. It can be seen the TiC particles are set within a dimensionally connected network structure, indicating the network structure as shown by XCT in the TiC preform has largely remained intact after infiltration by $NiAl_3$. The network of TiC particles appears to be set in horizontal layers, which is likely caused by the spreading of the powder during printing. Concerning the metallic matrix, there appears to exist two phases where a small, light grey area is set within the overall matrix and is more easily seen using a backscatter detector where elements with higher atomic number provide a brighter contrast. Therefore, the lighter regions are likely a more Ni-rich phase – possibly Ni_2Al_3. Closer inspection on the clusters of TiC revealed a darker phase that exists within the inter-particle area, which high contrast SEM revealed to be a mix of porosity and a darker matrix phase. EDS mapping of similar areas from another sample, shown in Fig. 8, revealed the dark inter-particle area to be rich in Al compared to the surrounding $NiAl_3$ base matrix. However, the area may also contain residual amounts of Ti, which might be a result of Ti leaching from the surrounding TiC particles. It is noteworthy that accurate quantitative EDS analysis within SEM of the darker areas was not possible given the high aerial density of surrounding TiC particles.

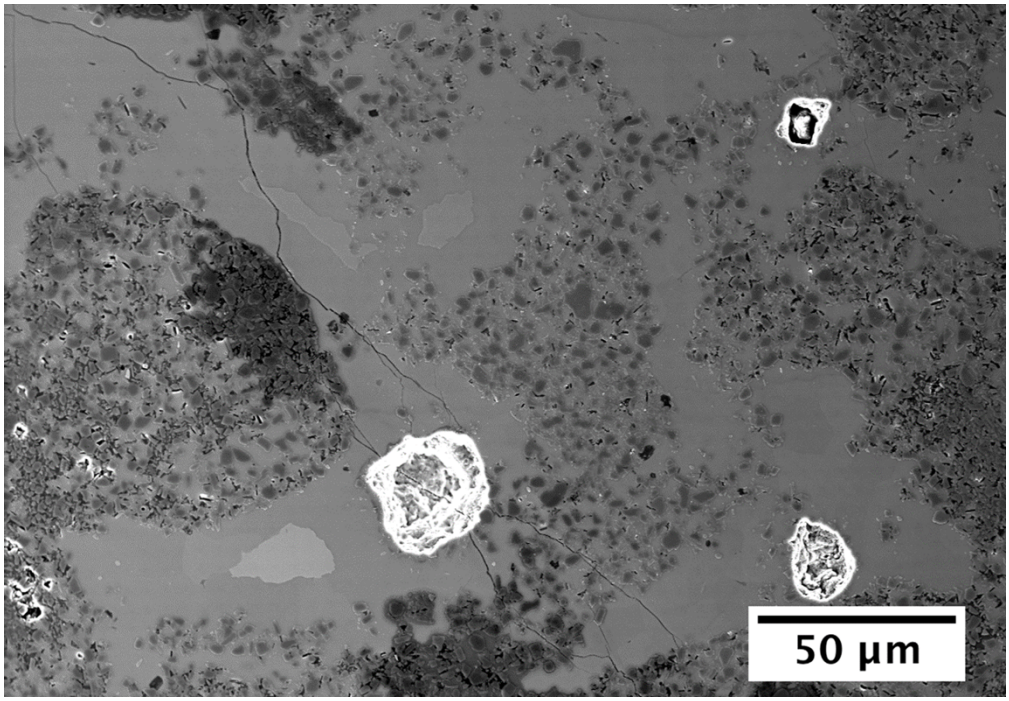

Figure 7. SEM in backscatter mode image of TiC preform infiltrated by $NiAl_3$ at 1415°C for 30 min. 500×.

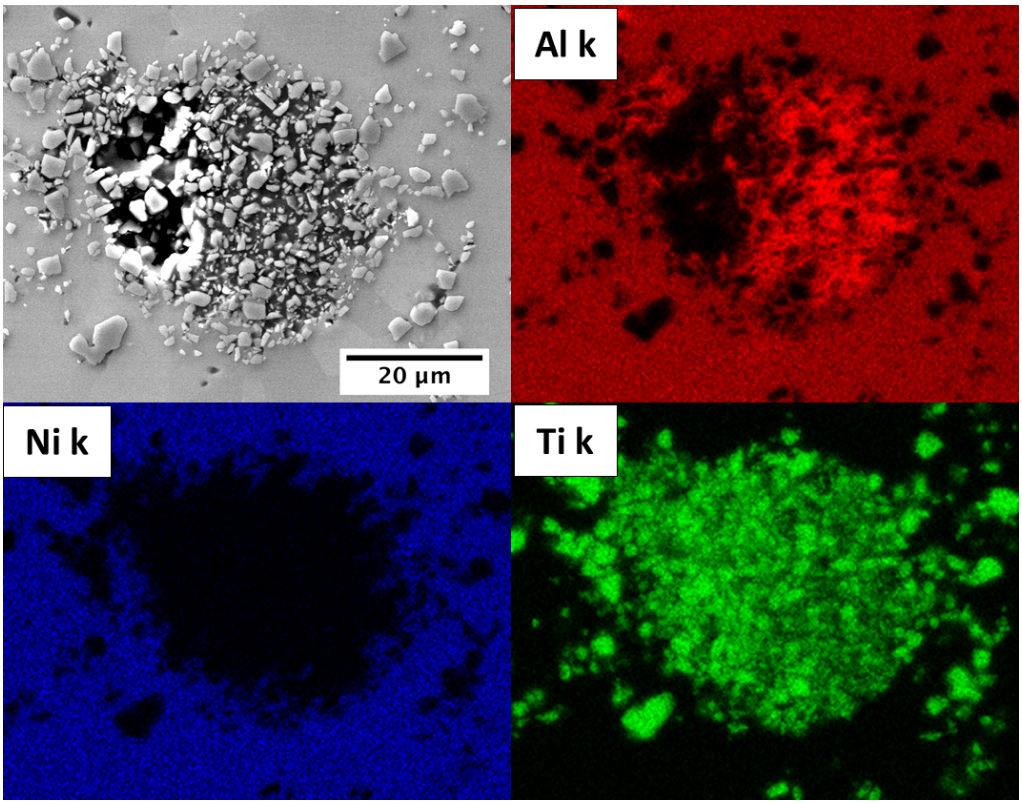

Figure 8. EDS mapping of TiC cluster in TiC preform infiltrated by NiAl3 at 1415°C for 30 min. Inter-particle area has Al-rich matrix phase with no detected Ni alongside porosity. 1,500×. Note: This map came from an identical sample with the additional of $NiAl_3$ in the cavity of the preform during infiltration, as well.

3.4 X-ray Diffraction of Samples

XRD was performed on the three samples from Table 1. Fig. 9 shows XRD of the samples where the bulk phases were detected. The TiC sample infiltrated with Ni_3Al at 1430°C for 30 min was comprised of TiC from the print, small amounts of NiAl from the infiltrant, and C from the conductive epoxy mount. The TiC sample infiltrated with Ni_3Al at 1430°C for 15 min was comprised of TiC from the print, NiAl from the infiltrant, and C from the conductive epoxy mount. The TiC sample infiltrated with $NiAl_3$ at 1415°C for 30 min was comprised of TiC from the print, NiAl from the infiltrant, $NiAl_3$ from the infiltrant, and C from the conductive epoxy mount. Al, Ni_3Al, and Ni_2Al_3 were not detected but may be present at interfaces where small amount of reaction occurs. It is likely that the Ni_3Al infiltrant reacted or decomposed to NiAl and other compositions during processing. The $NiAl_3$ infiltrant stayed $NiAl_3$ with some NiAl.

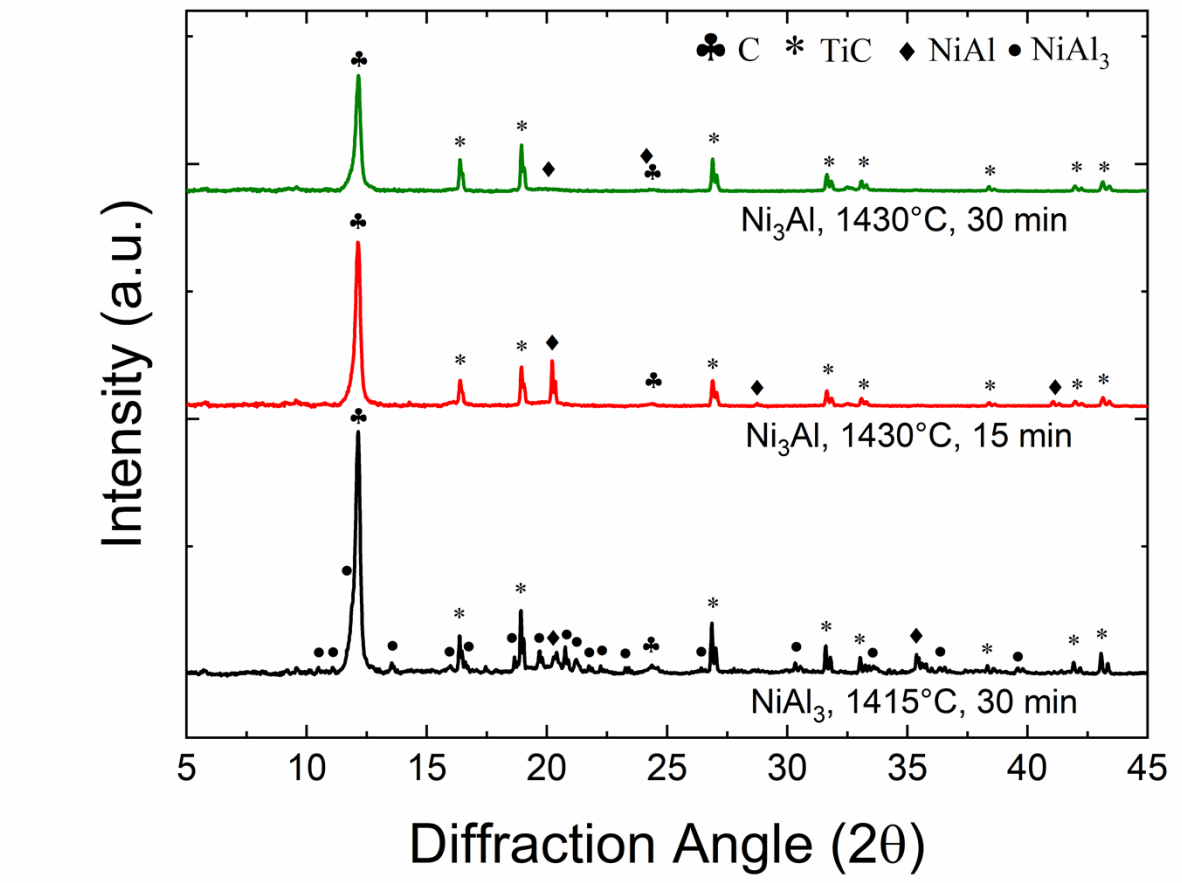

Figure 9. X-ray diffraction characterization of TiC preforms infiltrated with the two different intermetallic compositions with the conditions from Table 1. The data shows the different bulk phases that are detected after processing.

3.5 Detailed Evaluation of $NiAl_3$ Samples

In this section, the above observed macro and microstructural changes are analyzed further with computational tools and based on published literature related to melt infiltration. It is noteworthy that the infiltration behavior observed in $NiAl_3$ is expected. However, the microstructure evolution in $NiAl_3$ samples showed unusual behavior and, therefore, most of the evaluation focuses on these samples. First, the melting behavior of $NiAl_3$ should be confirmed to be consistent with published literature and thermodynamic calculations.

3.5.1 Evaluation of $NiAl_3$ Melting and Solidification Behavior

To investigate the peritectic behavior of $NiAl_3$ further and better understand the remnant material left after attempted infiltration of a TiC preform by $NiAl_3$, some $NiAl_3$ powder was melted separately without a TiC preform. Fig. 10 shows the melting result of $NiAl_3$, where clear separation of two distinct phases can be seen. The first phase is a dark, porous phase that was shown previously to remain after infiltration. The second phase is a shiny, metallic phase that exhibited a clear melting and solidification behavior. Qualitatively, the color of the metallic phase very closely matches the color of the infiltrated TiC preform presented earlier.

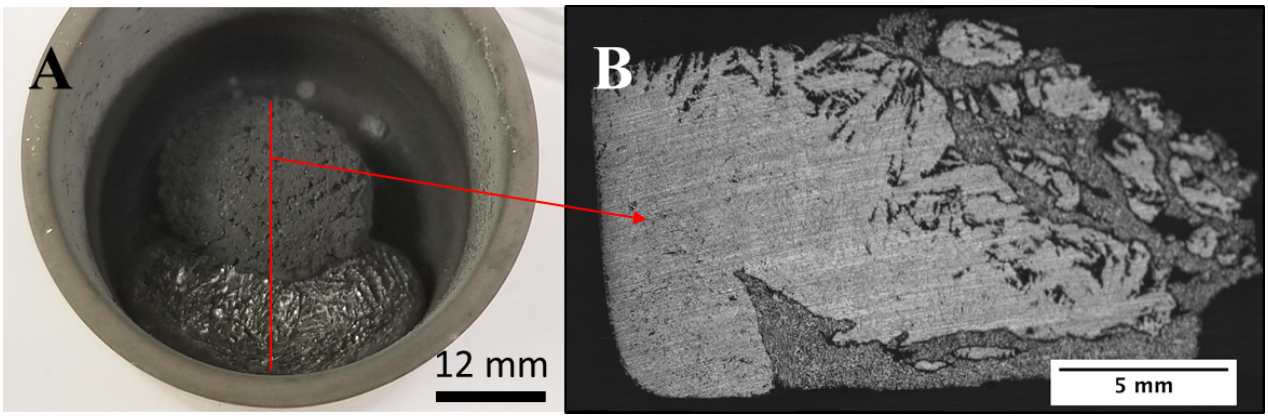

Figure 10. (A) Remnant material left in crucible after melting pure $NiAl_3$ powder. (B) Cross-section of segregated mixture.

Closer inspection of the shiny, metal phase by SEM (shown in Fig. 11) revealed a microstructure consisting of three distinct phases. Quantitative EDS measures the composition of each phase and showed the light grey regions to closely match the chemical composition of Ni_2Al_3, the grey regions to be the bulk composition of $NiAl_3$, and the darker areas to be ~99 at. % Al. Conversely, the dark porous macro phase appears to consist of the same phases but proved difficult to measure due to the highly porous nature of the microstructure.

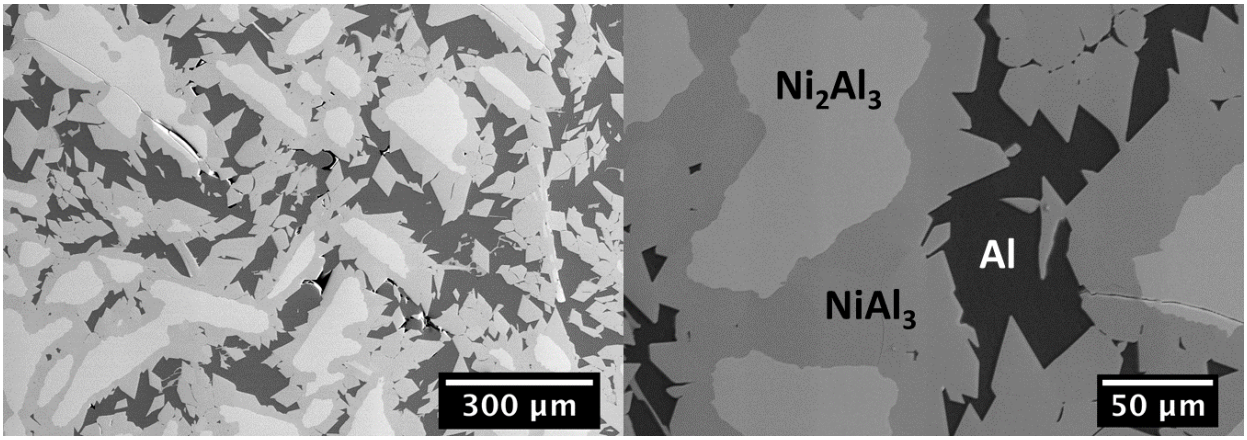

Figure 11. SEM of the microstructure showing three distinct phases: Ni_2Al_3 (light grey), $NiAl_3$ (grey), and Al (dark grey). (left) 100× and (right) 450×. These interpretations were purely based on the EDS analyses. It is noteworthy that X-ray diffraction failed to provide reliable diffraction patterns from these phases.

The Ni-Al phase diagram shown in Fig. 12 explains the peritectic melting and solidification behavior of $NiAl_3$, bulk composition set at 25 at. % Ni and marked. As $NiAl_3$ is heated, it will decompose to a mixture of solid Ni_2Al_3 + Al-rich liquid at ~820°C. With further heating, the amount of Al-rich liquid increases while being saturated in Ni. This will continue until ~1150°C, at which point the alloy becomes completely liquid with a bulk $NiAl_3$ composition. Upon cooling, Ni_2Al_3 will begin to nucleate and solidify, then $NiAl_3$, and finally the Al-rich liquid will reach the eutectic point at ~620°C (~0.03 at. % Ni) and FCC Al will nucleate alongside $NiAl_3$ in a possible eutectic structure. At the eutectic point, the structure is almost entirely Al with very minimal $NiAl_3$. Since the authors confirmed the evolution of microstructure in $NiAl_3$ is similar to

thermodynamic prediction, it is expected that similar microstructure evolution will occur after infiltration.

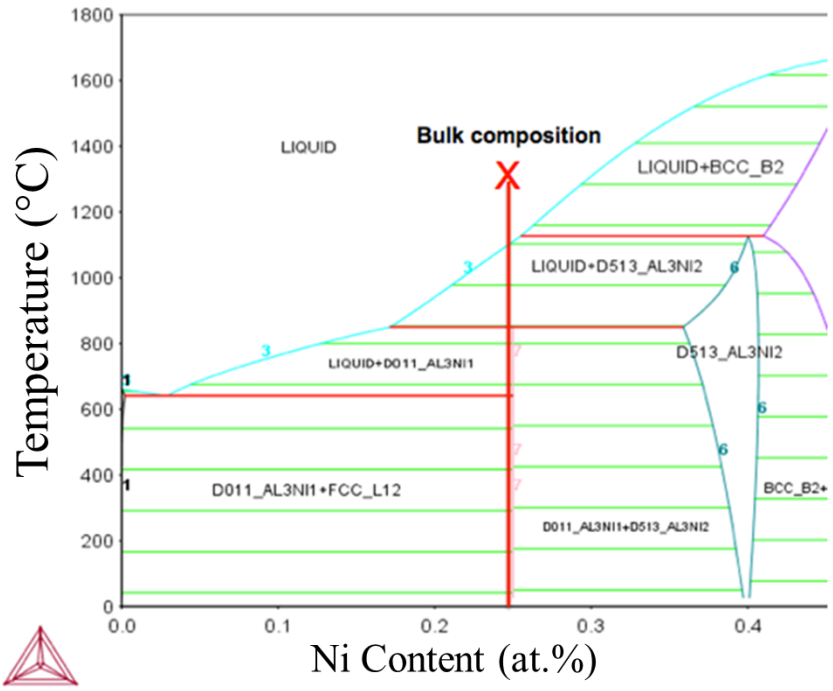

Figure 12. Ni-Al phase diagram constructed using ThermoCalc.

3.6 Dynamics of $NiAl_3$ Infiltration

As shown in Fig. 12, the peritectic behavior of $NiAl_3$ results in the segregation of an Al-rich liquid phase well before the soak temperature at 1415°C. For a "wetting" system, infiltration may be considered a spontaneous process where liquid, if present, will wick into a capillary at a fast rate via capillary action [34], [35]. If this Al-rich liquid wets TiC, the Al-rich liquid will potentially penetrate the TiC preform to some degree prior to the alloy fully melting. To investigate this further, $NiAl_3$ was infiltrated into a TiC preform (~50% dense) at 1000°C for 30 min. This soak temperature falls in the mixed solid and liquid phase field where the Al-rich liquid is ~88 at. % Al alongside solid Ni_2Al_3. Using the lever rule, the approximate amount of Al-rich liquid that should form was calculated to be ~75 wt.% of the total mixture, which was used to calculate the amount of infiltrant material necessary to fill the entire void space of the preform. The density of the liquid phase was assumed to be that of $NiAl_3$ (3.96g/cc), but the density was lower due to the increased Al content and required less overall material to fill the void space of the preform.

Fig. 13 shows the infiltration results where minimal to no infiltration of the TiC preform occurred, confirmed by weighing the preform before and after infiltration. Despite the lack of infiltration, the heavily segregated metallic phase shown previously to be rich in Al (similar to Fig. 11) indicates the melting behavior of the $NiAl_3$ powder. The matrix of the TiC infiltrated with $NiAl_3$ is mostly $NiAl_3$, but the segregated material could also be NiAl, according to XRD data. More investigation is needed to understand the interfaces and reactions occurring in this

system, as well, and more arduous analysis with diffraction data from transmission electron spectroscopy would help analyze small amount of phase around the TiC.

Figure 13. TiC preform infiltrated by $NiAl_3$ at 1000°C for 30 min. Material remnant (right) shows clear melting behavior and segregation of Al-rich phase.

4 Discussion

4.1 Rationalization of Poor Shape Retention During Ni_3Al Infiltration

Results show that attempted infiltration of a printed TiC preform by Ni_3Al resulted in a fully infiltrated, high density composite with poor shape retention. Microstructure of the infiltrated preform revealed the network structure of TiC particles present in the as-printed state largely gave way and evolved into a uniform dispersion of TiC within the Ni_3Al matrix. This is likely an indicator of strong TiC dissolution by liquid Ni_3Al, as also seen in the WC-Co system [36]. As liquid Ni_3Al infiltrates the TiC preform, the clusters of TiC are penetrated and broken up and result in the network structure dissolving away. It is likely that the matrix is NiAl, according to XRD, but further investigation of the matrix material and interfaces is needed. The reactions and interfaces are difficult to control when processing cermets with melt infiltration. The low green density (~30%) of the printed preform means there is more surface area per unit volume that may chemically interact with the advancing liquid infiltration front compared to a higher density preform.

4.2 Rationalization of Good Shape Retention During $NiAl_3$ Infiltration

Infiltration by the Al-rich $NiAl_3$ yielded a full, volumetrically infiltrated preform with excellent shape retention. The microstructure of the $NiAl_3$ infiltrated preform revealed the TiC network structure intact. The excellent shape retention after infiltration by $NiAl_3$ can be attributed to two mechanisms: 1) the dissolution of TiC by liquid $NiAl_3$ is less compared to Ni_3Al or 2) $NiAl_3$ reacts with TiC at the local interface through a metered infiltration to form a reaction product that might protect the TiC particles from further chemical interaction by the liquid infiltrant. Such a reaction might also provide a displacement reaction that might explain the apparent lack of shrinkage after infiltration by $NiAl_3$. These two hypotheses are evaluated below.

4.2.1 Sluggish Dissolution of TiC by $NiAl_3$

It is well-documented that liquid metal wets the carbides of transition metals (such as TiC) particularly well due to their mixed bonding characteristics [37], [38]. These carbides, such as TiC and WC, exhibit a mixed metallic-covalent-ionic bonding character dominated by metallic bonding at the interface. The nature of the mixed bonding of transition metal carbides is very complex but the metallic binding is a result of the electron transfer from carbon to the unfilled d-shell orbital of the base transition metal [38], [39]. When considering metals that wet TiC (and other transition metal carbides) favorably, transition metals with unfilled d-orbitals will react heavily to dissolve the carbide and form a solid solution [40]. Such metals include Fe, Ni, Co, Cr, Nb, Zr, and Ti. As such, it might be expected that the Ni-rich Ni_3Al would exhibit heavy dissolution of TiC and the more Al-rich $NiAl_3$ would react with TiC to a lesser degree, thereby leaving the TiC network structure intact after infiltration and maintaining the structural integrity of the printed preform. Unfortunately, there is no reported wetting angle of TiC by $NiAl_3$ in literature, but the reported wetting angles of Ni and Al on TiC can provide insight. As mentioned previously, transition metals (such as Ni) wet the carbides of transition metals (TiC) well, with a reported wetting angle as low as 25° for Ni on TiC. The wetting of TiC by Al is more complex, as it is a reactive system and exhibits dynamic wetting behavior. It is documented that aluminum experiences a non-wetting to wetting transition at elevated temperatures and will have a steadily decreasing contact angle over time by formation of Al_4C_3 at the interface with a reported equilibrium contact angle as low as 25–40° [39], [41]. This also indicates the potential for a dynamic wetting behavior of TiC by $NiAl_3$.

4.2.2 Metered Infiltration and Reactions

Despite the excellent shape retention after infiltration by $NiAl_3$, the infiltrated preform contains a significant amount of porosity and remnant infiltrant material is left in the crucible. The presence of remnant material in addition to a low infiltrated density (~88–90% TD) indicates that only partial infiltration of $NiAl_3$ occurs. Indeed, melting of $NiAl_3$ separately yields an Al-rich segregated macro-phase that has a clear three-phase microstructure containing Ni_2Al_3, $NiAl_3$, and FCC Al. The peritectic nature of $NiAl_3$ according to the Ni-Al phase diagram also predicts the formation of an Al-rich liquid phase well before the alloy has reached the fully liquid point. Segregation of the liquid phase as it forms would likely be in the form of "sweating," where small beads of liquid form on the surface of the powder. If this liquid wets TiC, there should be a driving force for infiltration into the preform that would occur well before the soak temperature has been reached.

Certainly, the capillaries present within the infiltrated preform are intuitively considered as open porosity within the overall TiC particle network structure, which measures to be ~20–40μm by image analysis. However, individual clusters of TiC particles may be a bundle of "micro" capillaries represented by the individual TiC particle spacing, measured to be ~0.1–1 μm. The size of the Al-rich liquid droplets that segregate from the powder by sweating would not be large enough to fill and wick into the larger capillaries of the TiC network structure but may wick into the micro capillaries between individual TiC particles. Despite the higher contact angle of a more Al-rich liquid, capillary pressure is inversely proportional to pore radius and, thus, the driving force for infiltration into the micro capillaries will be higher than for the macro capillaries of the TiC network. The infiltration of the micro capillaries between individual TiC particles by the Al-rich liquid would explain the high Al content measured within individual TiC clusters. In the

context of the TiC network structure, the Al-rich liquid would wick into the TiC network by way of micro capillaries without filling the void space of the preform. Previously, it was shown that no infiltration of the TiC preforms occurred at an intermediate temperature of 1000°C where the Al-rich liquid is present. However, if only small amounts of this Al-rich liquid were to infiltrate the micro capillaries of the preform, this might not be discernable in the overall mass of the preform after infiltration. As the liquid saturates in nickel with increasing temperature, the liquid may preferentially infiltrate the preform higher than 1000°C but prior to reaching the soak temperature.

Closer inspection of the $NiAl_3$ infiltrated microstructure revealed that TiC particles reside only within the $NiAl_3$ matrix while regions of Ni_2Al_3 are completely devoid of TiC particles. An example of this is shown in Fig. 14. Based upon the Ni-Al phase diagram, Ni_2Al_3 is the first phase to nucleate upon cooling from liquid and will continue to solidify over a large temperature range until the remaining Al-rich liquid eventually solidifies as $NiAl_3$ and finally Al. During cooling, solid TiC particles remain in the liquid and provide an existing solid-liquid interface upon which heterogeneous nucleation should occur. It would then be expected that Ni_2Al_3, as the first phase to solidify, would nucleate at the TiC interface and as the infiltrated preform is cooled, the Al-rich liquid at the Ni_2Al_3 interface would solidify as $NiAl_3$ and Al. Conversely, small amounts of NiAl B2 could form at the TiC interface. As the liquid with bulk composition $NiAl_3$ is cooled, the $NiAl_2$ B2 phase field falls within a single at. % of the liquidus point. If the liquid were slightly Ni-rich, solidification would begin with NiAl and the remaining liquid would then solidify as described above. For these two solidification theories, the matrix microstructure is compositionally graded such that most Ni-rich phases exist at the TiC particle interface and Al content rises with increasing distance from the local interface. However, the experimentally observed microstructure (Fig. 14) revealed that more Ni-rich phase Ni_2Al_3 exists away from the TiC interface, which cannot be explained by traditional solidification described by the Ni-Al phase diagram during cooling. The assumption with the described solidification theories is that a single liquid of bulk composition $NiAl_3$ has infiltrated the preform and undergone solidification by heterogeneous nucleation at the TiC interface. However, it was shown above that an Al-rich liquid that forms before the soak temperature may be infiltrating the micro capillaries of the TiC clusters prior to filling the void porosity. This metered infiltration process may occur due to the complex peritectic melting behavior of the $NiAl_3$ alloy and it is possible that a metered infiltration process could also occur within the macro capillaries of the preform.

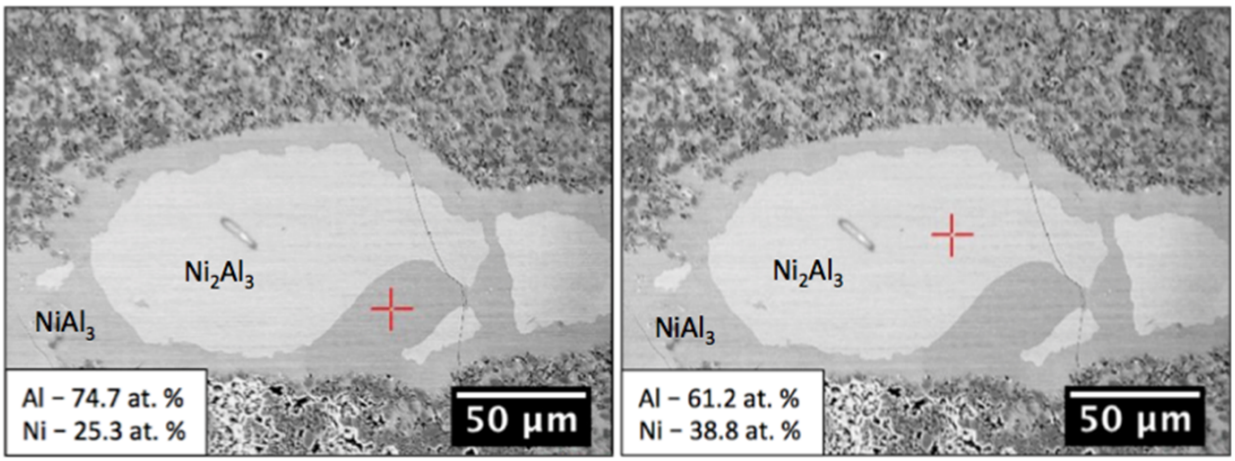

Figure 14. Quantitative EDS analysis of TiC preform infiltrated by $NiAl_3$ at 1415°C for 30 min. $NiAl_3$ is dark grey matrix phase. Ni_2Al_3 is lighter grey matrix phase.

At 850°C, $NiAl_3$ decomposes to a mixture of Ni_2Al_3 and Al-rich liquid. If this Al-rich liquid were to separate and infiltrate the preform first, then solid Ni_2Al_3 remains. Of course, segregation requires time and it is unlikely the composition has fully shifted during heating. With a bulk composition of the primary infiltrant material now closer to Ni_2Al_3, further heating to 1170°C will result in the decomposition of Ni_2Al_3 to a mixture of NiAl B2 solid and a liquid phase that is more Ni-rich than the original $NiAl_3$ infiltrant. If the "macro" capillaries of the preform have yet to be penetrated by the earlier Al-rich liquid, then this Ni-rich liquid could wick into the preform. The Al-rich liquid would then surround TiC clusters and the Ni-rich liquid would fill the remaining void space away from TiC. Upon cooling, solidification of the compositionally graded liquid results in the more Al-rich $NiAl_3$ phase surrounding the TiC particles and the Ni-rich Ni_2Al_3 existing at the $NiAl_3$ interface. Then, the remnant material in the crucible would be solid NiAl B2 that does not undergo melting during the infiltration process and experiences solid state decomposition to include $NiAl_3$ + Ni_2Al_3 and/or NiAl B2 and would explain why the remnant material after infiltration does not show a clear melting behavior.

5 Conclusions

The current research shows that the stability of TiC preforms, produced by binder jet additive manufacturing, differs to a large extent based on the composition of the Ni_xAl_y infiltrant. With the Ni_3Al composition, the preforms dissolved to a greater extent than with the $NiAl_3$ infiltrant. In contrast, the stability of the TiC preforms was good with the use of a $NiAl_3$ infiltrant. The potential mechanisms for this stability were evaluated through detailed microstructure evolution during melting and cooling of $NiAl_3$ with and without TiC preforms. The microstructure evolution of $NiAl_3$ was found to be different for these conditions. The $NiAl_3$ sample without preform showed phase separation of the Al-rich region due to progressive melting and separation as the sample melts and cools. The Ni-rich regions decomposed into composite (high melting point) Ni_2Al_3 phase encircled with (medium melting point) $NiAl_3$, followed by (low melting) Al regions. This microstructure evolution is indeed in agreement with thermodynamic calculations. Interestingly, the infiltrated regions of $NiAl_3$ showed a large difference in microstructure – the (medium melting point) $NiAl_3$ regions encircled Ni_2Al_3. This reversal in phase arrangement is

potentially attributed to sluggish dissolution of TiC by $NiAl_3$ or metered infiltration of the Al-rich region into the TiC preform on heating, which leads to cascading reactions during heating and cooling. In-situ phase analysis would be required to accurately determine the melting and solidification behavior of the alloy during infiltration, specifically for the phase progression of the infiltrant material as it segregates and wicks into and reacts with the TiC preform in addition to the solid-state phase transformation of the remnant material. Further, high-speed, in-situ video of the infiltration process would shed light on the kinetics of the $NiAl_3$ segregation and infiltration process.

6 Acknowledgements

The authors would like to acknowledge the support of the Center for Materials Processing at the University of Tennessee, A Tennessee Higher Education Commission (THEC) supported Accomplished Center of Excellence, for the use of various processing equipment to conduct parts of this research. The authors would also like to acknowledge Dr. John Salasin of the University of Tennessee, Knoxville for assistance with furnace runs; Dr. Ercan Cakmak and Dr. Tom Watkins of Oak Ridge National Lab for assistance with running XCT and XRD scans respectively; Derek Siddel and Desarae Goldsby of Oak Ridge National Lab for technical expertise and support on binder jet additive manufacturing; and Olivia Shafer for help with formatting and editing. This material is based upon work supported by the U.S. Department of Energy, Office of Energy Efficiency and Renewable Energy, Office of Advanced Manufacturing, under contract number DE-AC05-00OR22725.

7 References

[1] I. A. Ibrahim, F. A. Mohamed, and E. J. Lavernia, “Particulate reinforced metal matrix composites - a review,” *J. Mater. Sci.*, vol. 26, no. 5, pp. 1137–1156, 1991.

[2] N. Chawla and K. K. Chawla, *Metal Matrix Composites*. New York, NY: Springer New York, 2013.

[3] J. Davis, “No Title,” in *ASM Specialty Handbook: nickel, cobalt, and their alloys*, ASM International, 2000, pp. 104–105.

[4] C. T. Liu, R. W. Cahn, and G. Sauthoff, Eds., *Ordered Intermetallics — Physical Metallurgy and Mechanical Behaviour*. Dordrecht: Springer Netherlands, 1992.

[5] J. M. Yang, W. H. Kao, and C. T. Liu, “Development of Nickel aluminide matrix composites,” *Mater. Sci. Eng. A*, vol. 107, no. C, pp. 81–91, 1989.

[6] S. C. Deevi and V. K. Sikka, “Nickel and iron aluminides: An overview on properties, processing, and applications,” *Intermetallics*, vol. 4, no. 5, pp. 357–375, 1996.

[7] S. H. Whang, D. P. Pope, and C. T. Liu, Eds., “High Temperature Aluminides and Intermetallics,” in *Proceedings of the Second International ASM Conference on High Temperature Aluminides and Intermetallics*, 1991.

[8] R. Mitra, *Intermetallic Matrix Composites*. Elsevier Science & Technology, 2017.

[9] M. Ashby, “Designing architectured materials,” *Scr. Mater.*, vol. 68, no. 1, pp. 4–7, 2013.

[10] C. T. Liu and V. K. Sikka, “Nickel Aluminides for Structural Use _ _ _ _ _ _ _ _ _ _,” no. May, pp. 19–21, 1986.

[11] H. K. D. H. Bhadeshia, “Nickel Based Superalloys,” *University of Cambridge*. [Online].

Available: http://www.phase-trans.msm.cam.ac.uk/2003/Superalloys/superalloys.html. [Accessed: 02-Oct-2018].
[12] T. N. Tiegs and R. R. McDonald, "Ductile Ni3Al Alloys as Bonding Agents for Ceramic Materials," 4919718, 1990.
[13] K. Yamashita, I. Fujimoto, T. Murakumo, S. Kumai, and A. Sato, "Observation of glide dislocations in D020 ordered Al3Ni," *Philos. Mag. A*, vol. 80, no. 1, pp. 219–235, 2000.
[14] L. F. Mondolfo, *Aluminum Alloys: Structure and Properties*. 2013.
[15] V. K. Sikka, M. L. Santella, and C. T. Liu, "Processing, Properties, and Applications of Ni3Al-Based Alloys," 1997.
[16] T. N. Tiegs, K. B. Alexander, K. P. Plucknett, P. A. Menchhofer, P. F. Becher, and S. B. Waters, "Ceramic composites with a ductile Ni3Al binder phase," *Mater. Sci. Eng. A*, vol. 209, no. 1–2, pp. 243–247, 1996.
[17] B. Huang, W. Xiong, Q. Yang, Z. Yao, G. Zhang, and M. Zhang, "Preparation, microstructure and mechanical properties of multicomponent Ni3Al-bonded cermets," *Ceram. Int.*, vol. 40, no. 9 PART A, pp. 14073–14081, 2014.
[18] B. Huang, X. Tang, Y. Chen, H. Cheng, J. Yang, and W. Xiong, "High temperature oxidation behaviors of Ni3Al-bonded cermets," *J. Alloys Compd.*, vol. 704, pp. 443–452, 2017.
[19] Q. Shen, L. Zhang, and R. Tu, "Effect of Mo addition on the wettability between Ni3Al and TiC," *Key Eng. Mater.*, vol. 226, pp. 501–504, 2002.
[20] W. A. Sparling and K. P. Plucknett, "The effects of Mo2C additions on the sintering response of TiC0.3N0.7–Ni3Al cermets," *Int. J. Refract. Met. Hard Mater.*, vol. 61, pp. 98–106, 2016.
[21] K. P. Plucknett, P. F. Becher, and S. B. Waters, "Flexure Strength of Melt-Infiltrated-Processed Titanium Carbide/Nickel Aluminide Composites," *Ceram. Soc.*, vol. 44, pp. 1839–1844, 1998.
[22] P. F. Becher and K. P. Plucknett, "Properties of Ni3Al-bonded Titanium Carbide Ceramics," *J. Eur. Ceram. Soc.*, vol. 18, no. 4, pp. 395–400, 1998.
[23] Y. Pan and K. Sun, "Yi Pan 2000 upward melt infiltration.pdf," *J. Mater. Sci. Technol.*, vol. 16, no. 4, pp. 387–392, 2000.
[24] K. P. Plucknett and P. F. Becher, "Processing and Microstructure Development of Titanium Carbide – Nickel Aluminide Composites Prepared by Melt Infiltration / Sintering (MIS)," vol. 61, pp. 55–61, 2001.
[25] R. B. Collier and K. P. Plucknett, "Aqueous Processing of TiC Preforms for Advanced Cermet Preparation," in *Innovative Processing and Manufacturing of Advanced Ceramics and Composites*, Hoboken, NJ, USA: John Wiley & Sons, Inc., 2010, pp. 179–188.
[26] B. L. He and Y. F. Zhu, "Microstructure and properties of TiC/Ni3Al composites prepared by pressureless melt infiltration with porous TiC/Ni3Al preforms," *Mater. Manuf. Process.*, vol. 26, no. 4, pp. 586–591, 2011.
[27] M. B. Holmes, A. Ibrahim, G. J. Kipouros, Z. N. Farhat, and K. P. Plucknett, "The effects of Ni3Al binder content on the electrochemical response of melt-infiltration processed TiC–Ni3Al cermets," *Can. Metall. Q.*, vol. 55, no. 2, pp. 138–146, 2016.
[28] H. Liu, A. Wang, L. Wang, B. Ding, and Z. Hu, "In Situ Synthesis of TiC p / Ni 3 Al Composites under High Pressure," vol. 23, no. 191815, pp. 521–523, 1997.
[29] T. L. Stewart and K. P. Plucknett, "The sliding wear of TiC and Ti(C,N) cermets prepared with a stoichiometric Ni3Al binder," *Wear*, vol. 318, no. 1–2, pp. 153–167, 2014.

[30] X. Chen, J. Xu, Q. Sun, W. Yang, and W. Xiong, "Characterization of intermetallic bonded TiC composites prepared by mechanically induced self-sustained reaction," *Mater. Des.*, vol. 89, pp. 102–108, 2016.
[31] Z. Memarrashidi and K. P. Plucknett, "The influence of Ni3Al binder content on the aqueous corrosion response of TiC and Ti(C,N) cermets," *Int. J. Refract. Met. Hard Mater.*, vol. 64, pp. 113–121, 2017.
[32] A. M. Elliott, P. Nandwana, C. Shackleford, and C. K. Waters, "Roadmap for Metal Matrix Composite Development for Binder Jetting," *28th Annu. Int. Solid Free. Fabr. Symp. 2017*, 2017.
[33] M. X. Gao, Y. Pan, F. J. Oliveira, J. L. Baptista, and J. M. Vieira, "Microstructural characteristics of NiAl/TiC composites with high TiC content prepared by pressureless melt infiltration," *J. Mater. Sci.*, vol. 39, pp. 6385–6387, 2004.
[34] P. E. De Jongh and T. M. Eggenhuisen, "Melt infiltration: An emerging technique for the preparation of novel functional nanostructured materials," *Adv. Mater.*, vol. 25, no. 46, pp. 6672–6690, 2013.
[35] N. Eustathopoulos, "Wetting by Liquid Metals—Application in Materials Processing: The Contribution of the Grenoble Group," *Metals (Basel).*, vol. 5, no. 1, pp. 350–370, 2015.
[36] C. L. Cramer, P. Nandwana, R. A. Lowden, and A. M. Elliott, "Infiltration studies of additive manufacture of WC with Co using binder jetting and pressureless melt method," *Addit. Manuf.*, Apr. 2019.
[37] G. V. Samsonov, A. D. Panasyuk, and G. K. Kozina, "Wetting of Refractory Carbides," vol. 11, no. 11, pp. 874–878, 1968.
[38] W. S. Williams, "Physics of transition metal carbides," *Mater. Sci. Eng. A*, vol. 105–106, pp. 1–10, Nov. 1988.
[39] F. Delannay, L. Froyen, and A. Deruyttere, "The wetting of solids by molten metals and its relation to the preparation of metal-matrix composites composites," *J. Mater. Sci.*, vol. 22, no. 1, pp. 1–16, Jan. 1987.
[40] T. Y. Kosolapova, *Carbides: Propeties, Production, and Applications*. Boston, MA: Springer US, 1995.
[41] D. Muscat and R. A. L. Drew, "Modeling the infiltration kinetics of molten aluminum into porous titanium carbide," *Metall. Mater. Trans. A*, vol. 25, no. 11, pp. 2357–2370, 1994.